

# Unipolar nonvolatile memory devices based on the composites of poly(9-vinylcarbazole) and zinc oxide nanoparticles

Enming Zhao<sup>1</sup> · Diyou Liu<sup>1</sup> · Lu Liu<sup>1</sup> · Xinghua Yang<sup>1</sup> · Wei Kan<sup>2</sup> · Yanmei Sun<sup>3</sup>

Received: 13 January 2017 / Accepted: 17 April 2017 / Published online: 25 April 2017  
© Springer Science+Business Media New York 2017

**Abstract** The application of poly(9-vinylcarbazole) (PVK) to make a composite with zinc oxide (ZnO) as the active layer has been reported. Unipolar resistive switching behaviors were observed from ITO/PVK+ZnO/Al memory devices. The reset voltages were higher than the set voltages. These devices present a low resistance state (LRS)/high resistance state (HRS) current ratio of  $10^4$  when read at  $-0.5$  V, retaining the information for a time of  $10^5$  s. The bistable resistive switching behaviors were entirely steady within  $10^4$  cycles. The fitted results of  $I$ - $V$  curves shown that the dominant conduction mechanisms in LRS and HRS were Ohmic conductive behavior and space-charge-limited current mechanism, respectively.

## 1 Introduction

Organic devices have attracted a lot of attention on account of the significant advantages provided by organic materials and devices [1–4]. These advantages consist of low cost, high mechanical flexibility and versatility of the chemical structure. Particularly, organic memory devices using inorganic nanoparticles in the organic matrixes materials have been widely investigated because of easily controllable

processing factors like different kinds of particles, particle size, and concentration of particles [5–10]. In the kind of memory devices based on organic/inorganic nanocomposites, the electrical bistability is primarily determined by the inorganic nanoparticles [11–13]. The prospect of applications of nonvolatile memory devices utilizing hybrid inorganic/organic nanocomposites has given rise to extensive research and efforts to develop inorganic nanoparticles, serving as charging and discharging islands, embedded in a polymer matrix [11–13]. Among the various types of inorganic nanoparticles, zinc oxide (ZnO) have acted as promising candidates on account of their potential applications in next-generation nonvolatile memory devices and their being environment-friendly materials [14–18].

Although a lot of research based on ZnO nanoparticles/polymer composite systems have been reported [13, 19–22], where the characteristics were mostly bipolar resistive switching of memory nature, yet the unipolar electrical bistability have been relatively few. Nevertheless, unipolar resistive switching is more favorable than bipolar resistive switching memory, the unipolar memory could simplify the circuit design of memory devices [23, 24].

In this work, an electrically bistable memory device utilizing spin coating method was fabricated based on the nanocomposites of ZnO nanoparticles and poly(9-vinylcarbazole) (PVK). Current–voltage ( $I$ - $V$ ) curves were measured to investigate the electrical properties of the devices, and a large reproducible electrical bistability and unipolar resistive switching behavior was observed. The mechanism of resistive switching transformation was discussed.

✉ Enming Zhao  
zhaoem163@163.com

<sup>1</sup> Key Laboratory of In-fiber Integrated Optics, Ministry Education of China, Harbin Engineering University, Harbin 150001, People's Republic of China

<sup>2</sup> College of Chemistry and Chemical Engineering, Qiqihar University, Qiqihar 161006, People's Republic of China

<sup>3</sup> HLJ Province Key Laboratories of Senior-education for Electronic Engineering, Heilongjiang University, Harbin 150080, People's Republic of China

## 2 Experimental details

PVK was purchased from Sigma-Aldrich,  $M_w = 1,100,000$  g/mol, the ZnO nanoparticles that were used in this study were purchased from Hengqiu Graphene Technology (HGT) Co. Ltd (China). The average diameter and purity of the ZnO nanoparticles were 10 nm and 99.9%, respectively. The ITO glass were ultrasonically cleaned, successively, in deionized water acetone, and ethanol for 20 min at each step. The ZnO nanoparticles were dissolved in ethanol, and the dispersion was ultrasonicated for 1 h. Afterwards, the ZnO dispersion was blended with the previously filtered PVK solution (0.22 mm pore size filter) dissolved in chlorobenzene (10 mg/ml) and then ultrasonicated for 30 min. The composites were prepared with concentrations of 2, 5 and 10 wt% of ZnO. The memory devices with different ZnO content exhibited similar memory behaviors, and the memory devices with the lower ZnO concentration showed a better reproducibility and stability in their memory behavior. For this reason, in this work, all the memory devices have a 2 wt% of ZnO concentration in the active layer. Higher content of ZnO nanoparticle in PVK matrix is not conducive to the forming of active layer, so the stable and reproducible memory behavior in devices with low ZnO nanoparticles content may attributed to favorable uniformity and consistency of lower ZnO concentration ZnO nanoparticles in PVK matrix.

The mixed solution was deposited by the spin-coating method at 500 rpm for 12 s, then at 3000 rpm for 60 s. After spin coating, the film was baked on a hot plate at 60 °C for overnight. Afterwards, the top aluminum (Al) electrode was evaporated through a shadow mask. Figure 1 shows the schematic of the ITO/PVK + ZnO/Al device. Electrical characterization of the ITO/PVK + ZnO/Al devices was performed in ambient condition. The  $I$ - $V$  characteristics were measured by Keithley 4200 semiconductor parameter analyzer. The compliance current was set at 0.1 A. The contacts between the Al electrodes and the Keithley semiconductor parameter analyzer were made with nickel spring probes. Voltages were applied to top electrode (Al) with the bottom electrode (ITO) grounded the entire time.

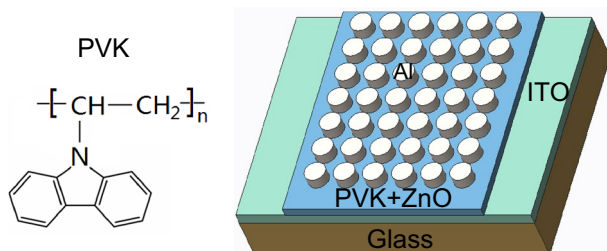


**Fig. 1** The schematic of the ITO/PVK + ZnO/Al device. *Inset* the chemical structure of PVK

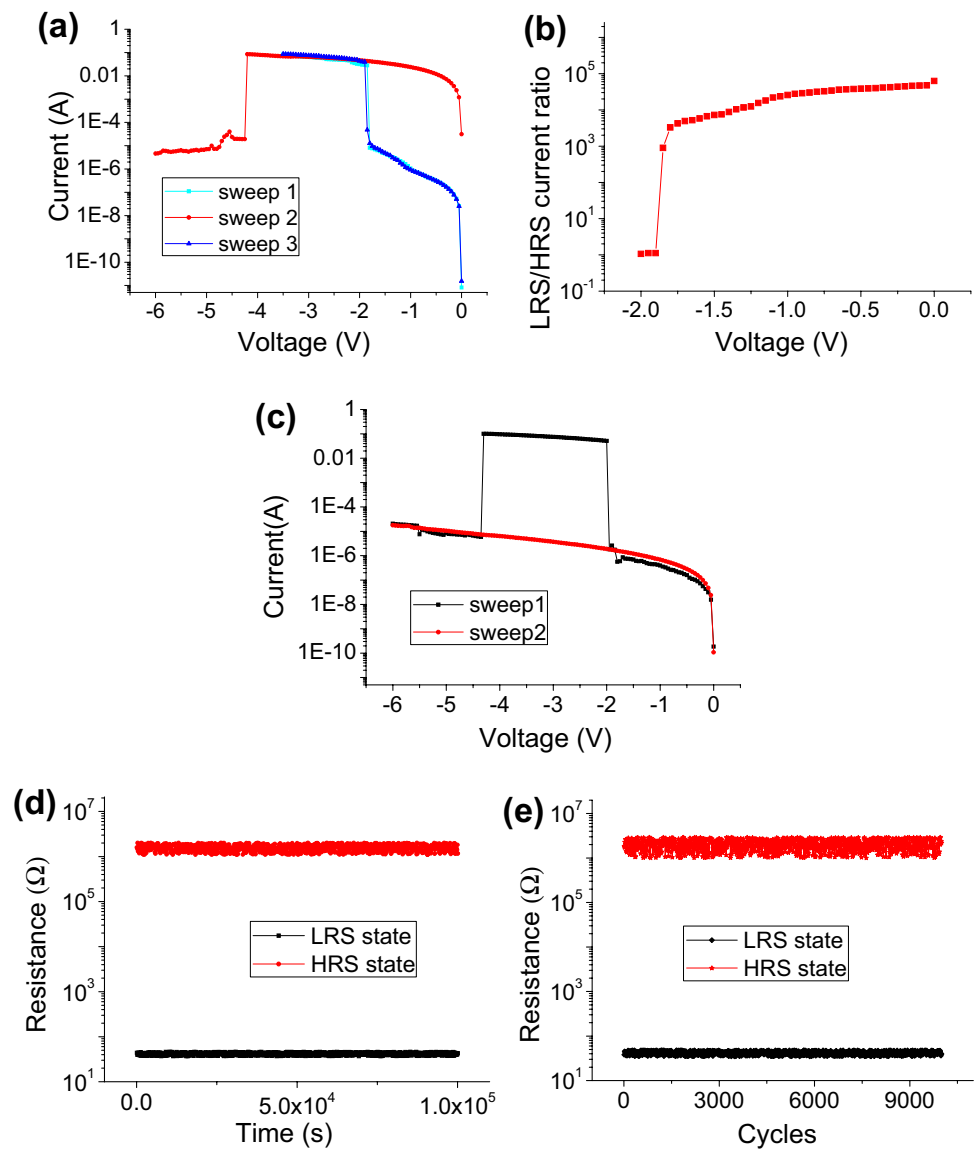
## 3 Result and discussion

The  $I$ - $V$  characteristics of ITO/PVK + ZnO/Al device was exhibited in semi-logarithmic plot in Fig. 2. At first, the pristine film was found to be insulating with resistance value of 2 M $\Omega$  (at  $-0.1$  V). Under negative voltage as shown in Fig. 2a, the current increases suddenly around  $-1.8$  V when the voltage was swept from 0 to  $-3.5$  V (sweep 1). This is known as the “set” switching process. After this process, the ITO/PVK + ZnO/Al device maintains at low resistance state (LRS) with a resistance of 42  $\Omega$ . When the voltage was swept from 0 to  $-6$  V (sweep 2), a rapid current drop was observed at a voltage of  $-4.2$  V manifesting a sudden resistance increase of the ITO/PVK + ZnO/Al device, and therefore, transformation of the ITO/PVK + ZnO/Al device from LRS to high resistance state (HRS). This is known as the “reset” process. The HRS was remained even then the applied voltage was removed. When the voltage was swept again from 0 to  $-3.5$  V (sweep 3), a sudden current increase was observed at  $-1.9$  V and the ITO/PVK + ZnO/Al device switched back into LRS. Thus, a repeatable nonvolatile unipolar resistive switching is demonstrated in ITO/PVK + ZnO/Al device. The HRS/LRS current ratio as a function of applied voltage in the negative sweep was shown in Fig. 2b, it is observed that a higher HRS/LRS current ratio of about  $3.3 \times 10^3$ – $6.3 \times 10^4$  in the range of 0 to  $-1.8$  V. When the sweep voltage in set process was enlarged to  $-6$  V, the  $I$ - $V$  characteristics as shown in Fig. 2c, a abrupt current increase was observed at  $-1.95$  V and then switched the ITO/PVK + ZnO/Al device from HRS to LRS, then followed by a abrupt current decrease at  $-4.35$  V converted the ITO/PVK + ZnO/Al device from LRS to HRS. No significant degradation of the device in both the LRS and HRS were observed after  $1.0 \times 10^5$  of the continuous stress test (Fig. 2d), indicating that the composite layers are stable. The endurance of the device has been performed up to  $10^4$  consecutive cycles, as shown in Fig. 2e. The well separated resistance values of LRS and HRS were read at  $-0.5$  V.

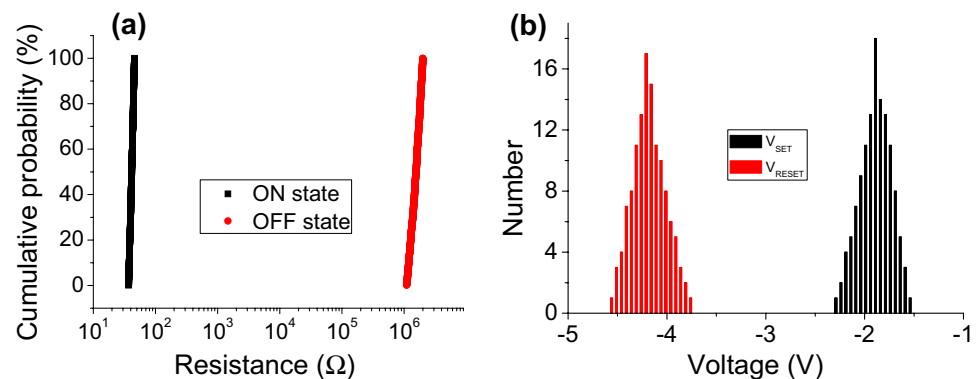
Figure 3a shows the statistical distribution of the resistance in LRS and HRS. Although each LRS and HRS was distributed over a wide resistance range, the important point is that the resistance of LRS were well separated from the HRS, indicating the memory margin was sufficient to distinguish each state. Figure 3b exhibits the histogram of the set and reset voltage. A narrow distribution of  $V_{SET}$  ( $-1.55$  to  $-2.3$  V), and  $V_{RESET}$  ( $-3.75$  to  $-4.55$ ) was obtained. About 2 V difference of two threshold switching voltage is observed between LRS and HRS, suggestive of a good repeatability and a clear identification between the two states.

Figure 4a shows the cross-section scanning electron microscopic (SEM) images of the PVK + ZnO composite

**Fig. 2** **a** Typical  $I$ - $V$  characteristic in semi-logarithmic scale of the ITO/PVK + ZnO/Al device showing resistive switching behavior. **b** The HRS/LRS current ratio as a function of applied voltage in the negative sweep. **c** The  $I$ - $V$  characteristics of the ITO/PVK + ZnO/Al device when the sweep voltage in set process was enlarged to  $-6$  V. **d** Retention characteristic of the ITO/PVK + ZnO/Al device with almost stable resistance values of HRS and LRS over a time period of  $10^5$  s. **e** The endurance of the ITO/PVK + ZnO/Al device over  $10^4$  consecutive cycles



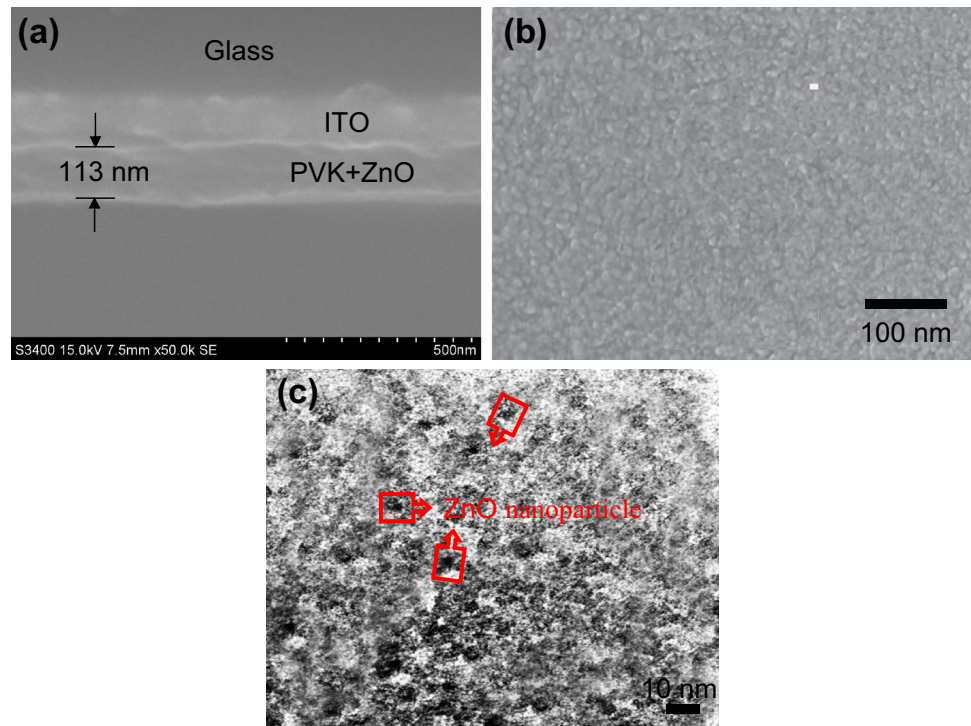
**Fig. 3** **a** Statistical distribution/cumulative probability of the resistance in HRS and LRS. **b** The statistical distribution of threshold voltages



films before the evaporation of Al electrode, from top to bottom the composition is glass, ITO film, and composite of PVK and ZnO layer. Figure 4b shows the surface morphology SEM image of PVK + ZnO composite

film. Figure 4c shows a transmission electron microscopy (TEM) image of PVK + ZnO composites. The ZnO nanoparticles are randomly distributed in the PVK layer.

**Fig. 4** **a** Cross-sectional SEM image of PVK + ZnO composite film. **b** Surface morphology SEM image of PVK + ZnO composite film. **c** Transmission electron microscopy image of PVK + ZnO composites



To clarify the conduction mechanism of the ITO/PVK + ZnO/Al device, the  $I$ – $V$  curves are re-plotted in double-log scale in Fig. 5. As can be seen in double logarithmic  $I$ – $V$  plot for HRS, three regimes were observed: one linear regimes (the slope of 1.14) for low voltages, and two non-linear regime for higher voltages, one for slope of 4.21, and other for slope of 19.99 where a quick increase in the current was observed. This kind of  $I$ – $V$  behavior can be understood by the trap-controlled space-charge-limited current conduction (SCLC) mechanism [25–27]. According to trap-controlled SCLC mechanism, the low voltage regime obeys Ohmic conduction, while in the intermediate voltage regime the conduction is complied with the Child's square law ( $I \sim V^2$ ), and the high voltage region corresponds to steep increase in current ( $I \sim V^\infty$ ). Our observed  $I$ – $V$  behavior in HRS was in better agreement with the trap-controlled

SCLC. Whereas, the  $I$ – $V$  relationship was found to be linear throughout the voltage range with slope of 1 indicating Ohmic conduction in LRS as shown in Fig. 5b. Hence, it can be inferred that the transition from the LRS to the HRS is a process of transition from a predominately Ohmic current to SCLC.

Carrier transport in the memory device based on composites of ZnO and polymer had been explained mostly by Fowler–Nordheim (FN) tunneling [28] and SCLC [20, 21, 29] as shown in Table 1. Kim et al. showed that the main conduction in Al/PS + ZnO/ITO followed SCLC by fitting the  $I$ – $V$  curves [20]. The conduction mechanism, however, in the cases of Al/PMMA + ZnO/ITO were obscure because it was just predicted as charge trapping without exact fitting of the log–log plot of the  $I$ – $V$  curves [13]. And the others of memory device based on composites of ZnO

**Fig. 5** **a**  $\log(I)$ – $\log(V)$  curve for HRS of ITO/PVK + ZnO/Al device showing three different regions in agreement with the trap-controlled SCLC conduction mechanism. **b**  $\log(I)$ – $\log(V)$  curve for LRS where the linear current–voltage relation indicates Ohmic conduction

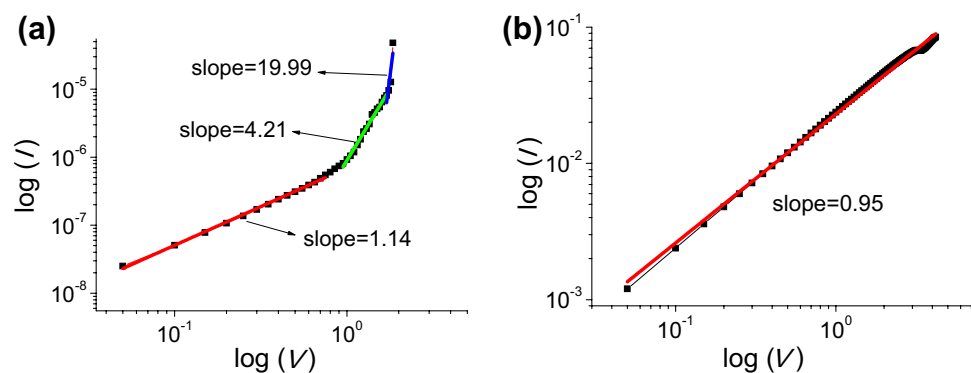


**Table 1** Charge transport mechanism of memory device based on composites of ZnO and polymer selected from the references

Structure	Polarity	Charge transport mechanism	Refs.
Al/PVK + ZnO/ITO	Unipolar	SCLC	This work
Al/PS + ZnO/ITO	Bipolar	SCLC	[20]
Al/PMMA + ZnO/ITO	Bipolar	SCLC	[21]
Al/PMMA + ZnO/ITO	Bipolar	Charge trapping	[13]
Al/PMMA + ZnO/ITO	Bipolar	Fowler–Nordheim tunneling	[8]
Al/PVP + ZnO/ITO	Bipolar	SCLC	[9]

nanoparticles and polymer as presented in Table 1, the carrier transport mechanism largely depends on the structure and electrical properties of the polymer matrix. It is noteworthy that compared with the Al/polymer + ZnO /ITO device, our Al/PVK + ZnO/ITO devices exhibit unipolar memory behavior.

Based on the analysis above, we explain the mechanism based on the formation and rupture of conduction pathways. In Al/PVK + ZnO/Al structure, the resistive switching is originated from the formation and rupture of the conduction pathways between two electrodes and composite layer due to the migration of oxygen ions [15]. When the negative voltage is applied to the top Al electrode, some oxygen atoms are pulled out of the lattice, generating oxygen vacancies. These oxygen ions will move toward the bottom ITO electrode and leave behind the tiny conducting filaments of oxygen vacancies in the composite layer. Subsequently, when the sweeping voltage reach the set voltage, those tiny conducting filaments gather speedily to form more conducting and stronger filaments leading to the device convert to the ON state. Then the charges can flow through the conductive pathways and sustain the device in an ON state. A large number of charges flow through the formed conduction pathways, and this process might produce an excess of heat. When the voltage bias exceeds a certain value, the number of injected charges will rise more than the capacity of the conduction pathways. The generated heat will cause rupture of the conduction channels formed in the reset process.

## 4 Conclusion

In summary, an electrically bistable ITO/PVK + ZnO/Al device was fabricated utilizing the composites of ZnO nanoparticles and PVK as active layers by a spin-coating method. The ITO/PVK + ZnO/Al device showed a remarkable electrical bistability and unipolar resistive switching effect in the current–voltage characteristics. The conduction mechanism turns from Ohmic-dominated to SCLC

model during the current conduction transition from the LRS to the HRS.

**Acknowledgements** This work is supported by the National Natural Science Foundation of China (NSFC, 61377085, 11574061, 61405043), Natural Science Foundation of Heilongjiang Province (F201338), the 111 project (B13015) to the Harbin Engineering University, and Fundamental Research Funds for the Central Universities.

## References

- X. Wang, W. Xie, J.-B. Xu, Graphene based non-volatile memory devices. *Adv. Mater.* **26**, 5496–5503 (2014)
- D.Y. Yun, T.W. Kim, Nonvolatile memory devices based on Au/grapheme oxide nanocomposites with bilateral multilevel characteristics. *Carbon* **88**, 26–32 (2015)
- C.-T. Poon, D. Wu, W.H. Lam, V.W.-W. Yam, A solution-processable donor-acceptor compound containing boron(III) centers for small-molecule-based high-performance ternary electronic memory devices. *Angew. Chem. Int. Ed.* **54**, 10569–10573 (2015)
- S. Qi, H. Iida, L. Liu, S. Irlle, W. Hu, E. Yashima, Electrical switching behavior of a [60]fullerene -based molecular wire encapsulated in a syndiotactic poly(methyl methacrylate) helical cavity. *Angew. Chem. Int. Ed.* **52**, 1049–1053 (2013)
- S. Coe, W.-K. Woo, M. Bawendi, V. Bulovic, Electroluminescence from single monolayers of nanocrystals in molecular organic devices. *Nature* **420**, 800–803 (2002)
- C.-J. Sun, Y. Wu, Z. Xu, B. Hu, J. Bai, J.-P. Wang et al., Enhancement of quantum efficiency of organic light emitting devices by doping magnetic nanoparticles. *Appl. Phys. Lett.* **90**, 232110 (2007)
- J.H. Shim, J.H. Jung, M.H. Lee, T.W. Kim, D.I. Son, A.N. Han et al., Memory mechanisms of nonvolatile organic bistable devices based on colloidal CuInS<sub>2</sub>/ZnS core-shell quantum dot-poly(N-vinylcarbazole). *Org. Electron.* **12**, 1566–1570 (2011)
- S.H. Kim, K.S. Yook, J.Y. Lee, J. Jang, Organic light emitting bistable memory device with high on/off ratio and low driving voltage. *Appl. Phys. Lett.* **93**, 053306 (2008)
- A. Tang, S. Qu, Y. Hou, F. Teng, H. Tan, J. Liu et al, Electrical bistability and negative differential resistance in diodes based on silver nanoparticle-poly(N-vinylcarbazole) composites. *J. Appl. Phys.* **108**, 094320 (2010)
- T.-Y. Chang, Y.-W. Cheng, P.-T. Lee, Electrical characteristics of an organic bistable device using an Al/Alq<sub>3</sub>/nanostructured MoO<sub>3</sub>/Alq<sub>3</sub>/p-Si structure. *Appl. Phys. Lett.* **96**, 043309 (2010)
- A.W. Tang, F. Teng, Y.B. Hou, Y.S. Wang, F.R. Tan, S.C. Qu et al., Optical properties and electrical bistability of CdS nanoparticles synthesized in dodecanethiol. *Appl. Phys. Lett.* **96**, 163112 (2010)
- CH.V.V. Ramana, M.K. Moodely, V. Kannan, A. Maity, J. Jayaramudu, W. Clarke, Fabrication of stable low voltage organic bistable memory device. *Sens. Actuators B* **161**, 684–688 (2012)
- D.T. Thanh, T.T. Viet, H. Koichi, O. Hiromasa, D. Mott, S. Maenosono et al., High-performance nonvolatile write-once-read-many-times memory devices with ZnO nanoparticles embedded in polymethylmethacrylate. *Appl. Phys. Lett.* **99**, 233303 (2011)
- R.N. Koteeswara, M. Devika, C.W. Tu, Vertically aligned ZnO nanorods on flexible substrates for multifunctional device applications: easy and cost-effective route. *Mater. Lett.* **120**, 662–664 (2014)
- A. Kathalingam, H.-S. Kim, S.-D. Kim, H.-M. Park, H.-C. Park, Unipolar resistive switching of solution synthesized ZnO

- nanorod with self-rectifying and negative differential resistance effects. *Mater. Lett.* **142**, 238–241 (2015)
16. S. Paul, P.G. Harris, C. Pal, A.K. Sharma, A.K. Ray, Low cost zinc oxide for memristors with high on-off ratios. *Mater. Lett.* **130**, 40–42 (2014)
  17. B. Sun, W. Zhao, L. Wei, H. Li, P. Chen, Enhanced resistive switching effect upon illumination in self-assembled NiWO<sub>4</sub> nano-nests. *Chem. Commun.* **50**, 13142–13145 (2014)
  18. B. Sun, C.M. Li, Light-controlled resistive switching memory of multiferroic BiMnO<sub>3</sub> nanowire arrays. *Phys. Chem. Chem. Phys.* **17**, 6718–6721 (2015)
  19. J.H. Jung, J.Y. Jin, I. Lee, T.W. Kim, H.G. Roh, Y.-H. Kim, Memory effect of ZnO nanocrystals embedded in an insulating polyimide layer. *Appl. Phys. Lett.* **88**, 112107 (2006)
  20. D.Y. Yun, J.K. Kwak, J.H. Jung, T.W. Kim, D.I. Son, Electrical bistabilities and carrier transport mechanisms of write-once-read-many-times memory devices fabricated utilizing ZnO nanoparticles embedded in a polystyrene layer. *Appl. Phys. Lett.* **95**, 143301 (2009)
  21. D.-I. Son, D.-H. Park, W.K. Choi, S.-H. Cho, W.-T. Kim, T.W. Kim, Carrier transport in flexible organic bistable devices of ZnO nanoparticles embedded in an insulating poly(methyl methacrylate) polymer layer. *Nanotechnology* **20**, 195203 (2009)
  22. Z.-X. Xu, V.A.L. Roy, P. Stallinga, M. Muccin, S. Toffanin, H.-F. Xiang, C.-M. Che, Nanocomposite field effect transistors based on zinc oxide/polymer blends. *Appl. Phys. Lett.* **90**, 223509 (2007)
  23. S. Sarma, B.M. Mothudi, M.S. Dhlamini, Unipolar resistive switching behavior of copper doped polyvinyl alcohol/lead sulphide quantum dot device. *J. Mater. Sci. Mater. Electron* **27**, 3785–3790 (2016)
  24. W.Y. Chang, Y.C. Lai, T.B. Wu, S.-F. Wang, F. Chen, M.-J. Tsai, Unipolar resistive switching characteristics of ZnO thin films for nonvolatile memory applications. *Appl. Phys. Lett.* **92**, 022110 (2008)
  25. Q. Liu, W. Guan, S. Long, R. Jia, M. Liu, J. Chen, Resistive switching memory effect of ZrO<sub>2</sub> films with Zr<sup>+</sup> implanted. *Appl. Phys. Lett.* **92**, 012117 (2008)
  26. J.H. Shim, J.H. Jung, M.H. Lee, T.W. Kim, D.I. Son, A.N. Han et al., Memory mechanisms of nonvolatile organic bistable devices based on colloidal CuInS<sub>2</sub>/ZnS core-shell quantum dot-poly(N-vinylcarbazole) nanocomposites. *Org. Electron.* **12**, 1566–1570 (2011)
  27. H. Wang, F. Meng, B. Zhu, W.R. Leow, Y. Liu, X. Chen, Resistive switching memory devices based on proteins. *Adv. Mater.* **27**, 7670–7676 (2015)
  28. D.I. Son, C.H. You, W.T. Kim, J.H. Jung, T.W. Kim, Electrical bistabilities and memory mechanisms of organic bistable devices based on colloidal ZnO quantum dot-polymethylmethacrylate polymer nanocomposites. *Appl. Phys. Lett.* **95**(2009), 132103 (2009)
  29. C.W. Lin, T.S. Pan, M.C. Chen, Y.J. Yang, Y. Tai, Y.F. Chen, Organic bistable memory based on Au nanoparticle/ZnO nanorods composite embedded in poly (vinylpyrrolidone) layer. *Appl. Phys. Lett.* **99**, 023303 (2011)